PNAS RESEARCH ARTICLE | CHEMISTRY

Anomalously enhanced ion transport and uptake in functionalized angstrom-scale two-dimensional channels

Mingzhan Wang[a], Tumpa Sadhukhan[b,c], Nicholas H. C. Lewis[d], Maoyu Wang[e], Xiang He[f,1], Gangbin Yan[a], Dongchen Ying[a], Eli Hoenig[a], Yu Han[a], Guiming Peng[a,2], One-Sun Lee[b], Fengyuan Shi[g], David M. Tiede[f], Hua Zhou[e], Andrei Tokmakoff[d], George C. Schatz[b,3], and Chong Liu[a,3]

Contributed by George C. Schatz; received August 20, 2023; accepted December 1, 2023; reviewed by De-en Jiang and Young-Shin Jun

Emulating angstrom-scale dynamics of the highly selective biological ion channels is a challenging task. Recent work on angstrom-scale artificial channels has expanded our understanding of ion transport and uptake mechanisms under confinement. However, the role of chemical environment in such channels is still not well understood. Here, we report the anomalously enhanced transport and uptake of ions under confined MoS_2-based channels that are ~five angstroms in size. The ion uptake preference in the MoS_2-based channels can be changed by the selection of surface functional groups and ion uptake sequence due to the interplay between kinetic and thermodynamic factors that depend on whether the ions are mixed or not prior to uptake. Our work offers a holistic picture of ion transport in 2D confinement and highlights ion interplay in this regime.

nanofluidics | 2D channels | ion transport | ion interplay | confinement chemistry

Significance

Under angstrom-scale confinement, matter behaves differently from the bulk. Exploring fundamental ion transport laws in this regime not only pushes our understanding but also provides guidelines for building ion-based devices that are important in water purification and ion separation. Here, we observed that under chemically modified 2D confinement, anomalously enhanced ion transport arises from the ion-channel interactions and that the interplay between the kinetics and thermodynamics of ion uptake leads to a flipped ion uptake sequence for ion mixtures. Our work shows promise for using synthetic tools to enable designable mass transport properties using angstrom-scale confinement.

Biological ion channels represent intriguing examples of fast and selective ion transport in molecular scale structures (1). Realizing their synthetic counterparts will significantly impact many fields including energy conversion (2–4), water purification (5), and emerging ionotronics (6, 7). Structural studies have established that the selectivity filters in biological channels typically feature characteristic dimensions of several angstroms (Å) and fine-tuned chemistry. For example, the potassium ion (K^+) channel, KcsA, has a selectivity filter of several angstrom in dimension built from carbonyl groups, showing over 10^4-fold K^+/Na^+ selectivity and close-to-limiting conductivity of K^+ (up to 10^8 ions per second) (8–10). In addition to widely investigated one-dimensional (1D) (11–13) and nanoporous materials (14–16), the emergence of two-dimensional (2D) materials (including graphene, hexagonal boron nitride (h-BN), metal chalcogenides, and MXenes) opens new opportunities for creating artificial channels at the angstrom-scale or even down to single-atom layer, similar in dimension to the selectivity filters in biological ion channels (17–21). In artificial channels, size sieving is mostly utilized to promote ion selectivity since the confinement dimension is comparable to the size of water molecules and hydrated ions. For example, graphite or h-BN 2D channels with heights of ~3.4 Å (using monolayer graphene as the spacer) can accommodate only a monolayer of water and show clear sieving effects such that they conduct protons efficiently while totally rejecting other ions like Na^+, K^+, Mg^{2+}, and Ca^{2+} (19). However, when the confinement is relaxed to ~6.6 Å (using monolayer MoS_2 or bilayer graphene as the spacer), not only can Na^+, K^+, Mg^{2+}, and Ca^{2+} pass through, but also larger ions such as Fe^{3+}, In^{3+}, and Al^{3+} (*SI Appendix*, Table S1), although the underlying dehydration effect drastically decreases their mobilities (18).

Beyond dimension, the chemical environment in confinement is largely unexplored in artificial channels, unlike K^+ channels (22), since exfoliated 2D crystals like graphite and h-BN bear neither charge nor any functional groups on their basal planes (18). Moreover, possible exotic transport properties due to ion interplay under 2D confinement remain unknown. Here, we create a precise chemical environment in confined 2D channels by anchoring carboxylic acid groups onto MoS_2 and unveil their defining effect on selective ion transport. Pb^{2+}, in a mixture of seventeen cations, shows drastically enhanced transport and highest uptake in the presence of carboxylate groups, even though Cu^{2+} shows the largest uptake in a single salt uptake experiment. Both thermodynamic and kinetic factors contribute to these results. For thermodynamics, covalent Cu–S interactions that are missing for other ions lead to the highest binding energy for Cu^{2+}; and the bidentate binding of Pb^{2+} to carboxylate functional groups favors Pb^{2+} uptake for all ions except Cu^{2+}. For kinetics, with lower activation energies and a faster rate for Pb^{2+} to enter the channels (as a result of a weak hydration), Pb^{2+} can define (i.e., "lock") the interlayer spacing in the presence of ion mixtures, which leads to expelling of most other ions, with Pb^{2+} dominating transport.

To survey the landscapes of ion transport under confinement as completely as possible, we designed a competitive permeation experiment, as schematically illustrated in Fig. 1*A*

Author contributions: Mingzhan Wang, G.C.S., and C.L. designed research; Mingzhan Wang, T.S., N.H.C.L., Maoyu Wang, X.H., G.Y., D.Y., Y.H., O.-S.L., F.S., D.M.T., H.Z., A.T., and C.L. performed research; Mingzhan Wang, T.S., N.H.C.L., Maoyu Wang, X.H., E.H., G.P., D.M.T., H.Z., A.T., and G.C.S. analyzed data; and Mingzhan Wang, T.S., G.C.S., and C.L. wrote the paper.

Reviewers: D.-e.J., University of California Riverside; and Y.-S.J., Washington University in St. Louis.

The authors declare no competing interest.

[1]Present address: Department of Mechanical and Civil Engineering, Florida Institute of Technology, Melbourne, FL 32901.

[2]Present address: College of Chemistry and Chemical Engineering, Jiangxi Normal University, Nanchang, Jiangxi 330022, China.

[3]To whom correspondence may be addressed. Email: g-schatz@northwestern.edu or chongliu@uchicago.edu.

This article contains supporting information online at https://www.pnas.org/lookup/suppl/doi:10.1073/pnas.2313616121/-/DCSupplemental.

Published January 2, 2024.

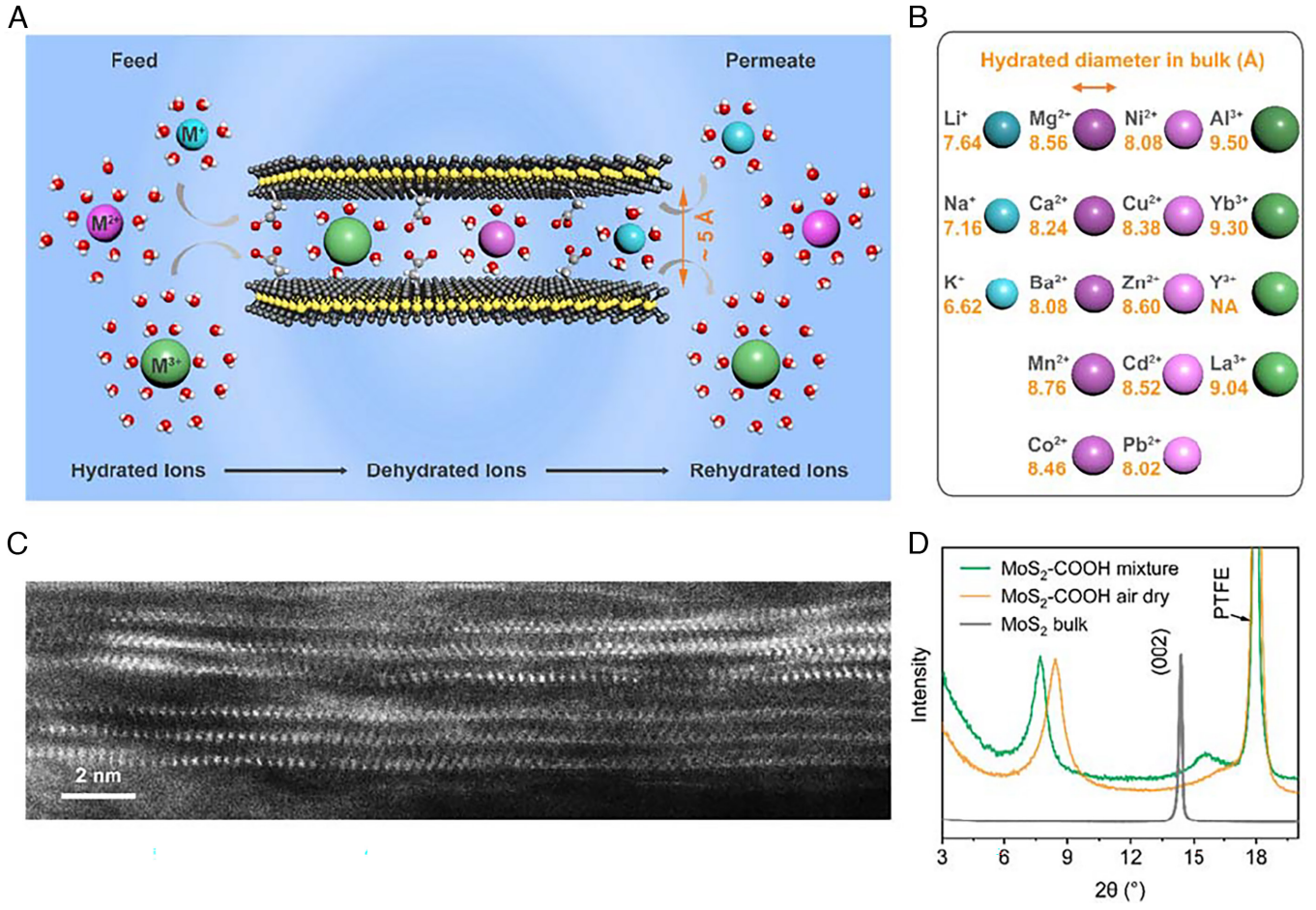

Fig. 1. Artificial angstrom-scale 2D ion channels. (*A*) Schematic of the competitive permeation test of mixed ions through MoS_2-based angstrom-scale 2D channels. The anions (either pure nitrate or mixed chloride/nitrate) are omitted for clarity. The hydrated ions go through dehydration processes when going through the confined 2D channels. (*B*) The selected seventeen cations in the mixture and their corresponding hydrated diameters (23) (see details in *SI Appendix*, Table S1). (*C*) Cross-section STEM image of MoS_2-COOH membrane showing the 2D channels in the dry state. (*D*) XRD spectra of bulk MoS_2 and MoS_2-COOH membranes in both the air-dry state without any ion and the wet state in the mixture solution.

and *SI Appendix*, Fig. S1. A mixture solution of seventeen metal cations of the same concentration (~4 mM, total ionic strength ~228 mM, *SI Appendix*, Fig. S2) is used as the feed, and deionized water (DIW) of the same volume is used as the permeate with the membrane constructed by 2D angstrom-scale channels mounted in-between. The permeation rates of individual ions as determined by their chemical potential gradients, i.e., from the feed to the permeate, are measured and the diffusion coefficients are calculated accordingly. The selection principle for choosing these mixed metal cations is to be as diverse, representative, and compatible as possible. To that end, we include monovalent ($Li^+/Na^+/K^+$), divalent ($Mg^{2+}/Ca^{2+}/Mn^{2+}/Co^{2+}/Ni^{2+}/Cu^{2+}/Zn^{2+}/Cd^{2+}/Ba^{2+}/Pb^{2+}$), and trivalent ($Al^{3+}/Y^{3+}/La^{3+}/Yb^{3+}$) cations (Fig. 1*B*). All the metal cations have the same initial molarity in the feed and are exposed to the same environment, *e.g.,* temperature, pressure, membrane condition, and osmotic pressure.

The model 2D channels are built by restacking acetic acid-functionalized MoS_2 (denoted as MoS_2-COOH hereafter) or pristine MoS_2 without functionalization (*SI Appendix*, Fig. S3, functionalization, and membrane fabrication details in *SI Appendix*). The carboxylic acid group (-COOH) was chosen to explore the role of surface chemistry in ion transport due to its coordination capability with cations. Also, the covalently bonded carboxylate groups can realize the controlled and uniform hydration of the MoS_2-COOH membrane (24), which otherwise cannot be achieved for the pristine MoS_2 membrane itself (25, 26). Fig. 1*C* shows a typical cross-section scanning transmission electron microscopy (STEM) image of the layered structure of the restacked MoS_2-COOH membrane in its dry state. X-ray diffraction (XRD) spectra (Fig. 1*D*) show that the interlayer spacing of the pristine MoS_2-COOH membrane in its dry state is ~10.5 Å, larger than that of bulk crystalline MoS_2 (~6.2 Å). The value increases to ~11.4 Å in the mixture solution. The pristine MoS_2 membrane shows a similar interlayer spacing in the mixture solution (~11.3 Å, *SI Appendix*, Fig. S3). By deducting the intrinsic thickness of a monolayer MoS_2 sheet (~6.2 Å), the effective channel heights for transport of the mixed ions in the MoS_2-COOH membrane and the MoS_2 membrane are ~5.2 Å and 5.1 Å, respectively, implying a bilayer-water structure in the channels.

Anomalous Ion Transport

The identification and quantification of individual cations in both the feed and the permeate are accomplished using inductively coupled plasma mass spectrometry (ICP-MS). The concentration changes of all cations over time are simultaneously monitored by periodic samplings. Quantitative analyses are made based on the permeation rates, $\boldsymbol{P}_i$ (mol/s), and the extracted effective diffusion coefficients, $\boldsymbol{D}_{eff\text{-}i}$ (cm^2/s), of the permeated cations across the membranes (calculation details in the *SI Appendix*). K^+ is used as reference. The relative ion permeation rates, $\boldsymbol{P}_i/\boldsymbol{P}_{K^+}$, across the MoS_2-based membranes and bare commercial porous hydrophilic

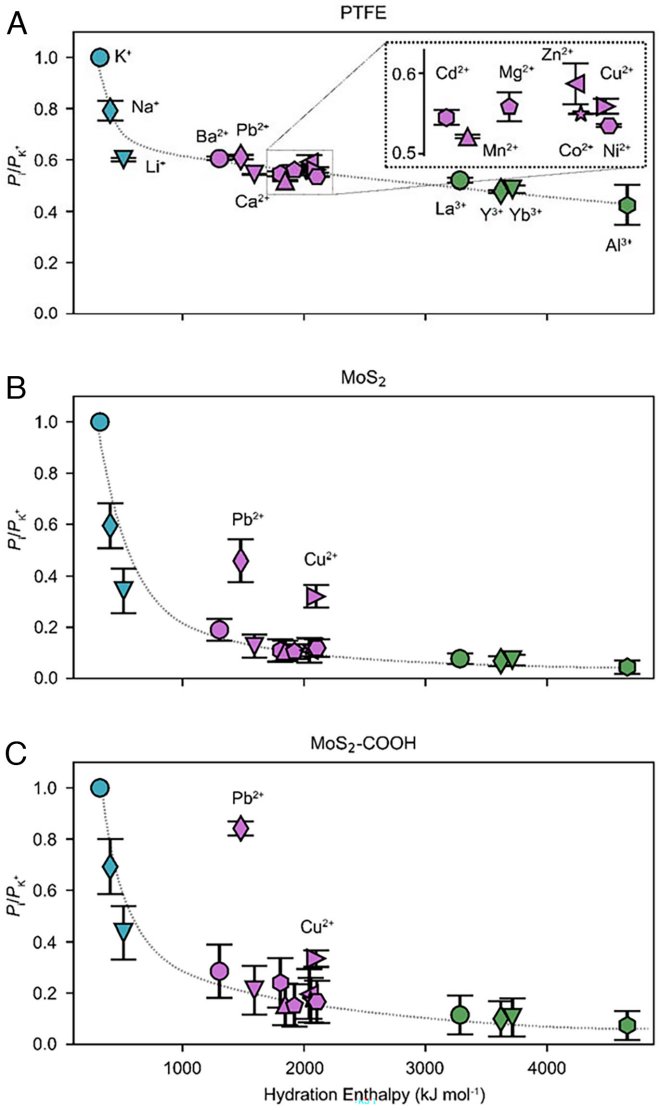

Fig. 2. Ion transport across the 2D channels. (*A–C*) The relative ion permeation rates versus their hydration enthalpies across the PTFE membrane, the pristine MoS_2 membrane, and the MoS_2-COOH membrane, respectively. The dashed lines are guidelines. Mixture: ~4 mM, Cl^-/NO_3^- (~96 mM:44 mM) anions, pH ~ 4.13.

polytetrafluoroethylene (PTFE) membrane (substrate with average pore size ~200 nm) are shown in Fig. 2 *A–C* and *SI Appendix*, Fig. S4. $\boldsymbol{P}_i/\boldsymbol{P}_{K^+}$ values are plotted against the hydration radii and hydration enthalpies of the ions (*SI Appendix*, Table S1), both of which characterize the interactions between ions and water molecules within their hydration shells.

For the bare PTFE membrane, the cations show a generally decreasing trend in the transport rate with increasing hydration enthalpy and hydration radius (Fig. 2*A* and *SI Appendix*, Fig. S5). This is not surprising because larger hydration radius and hydration enthalpy (i.e., stronger Lewis acidity of cations) imply stronger interactions between ions and water molecules within their hydration shells. So, the monovalent cations show the largest $\boldsymbol{P}_i$, followed by divalent cations, and trivalent cations show the smallest $\boldsymbol{P}_i$. We note that the calculated values of the effective diffusion coefficient $\boldsymbol{D}_{eff\text{-}i}$ across the PTFE exhibit a trend fully consistent with those of the tabulated bulk diffusion coefficients (*SI Appendix*, Fig. S5 *E–H*). This suggests that the large pores of ~200 nm exert neither a spatial confinement effect nor selectivity toward hydrated cations.

By comparison, there are two distinct features of the MoS_2-based membranes that are not present in the PTFE membrane (Fig. 2 *B* and *C* and *SI Appendix*, Figs. S6 and S7). First, Pb^{2+} and Cu^{2+} are unambiguous outliers in the plots, exhibiting anomalously enhanced $\boldsymbol{P}_i$, and Pb^{2+} is more enhanced in the MoS_2-COOH membrane than in the pristine MoS_2 membrane. Second, all ions except Pb^{2+} and Cu^{2+} show a more pronounced decrease of $\boldsymbol{P}_i$ with the increase in hydration radii and hydration enthalpies in the MoS_2-based membranes than in the PTFE membrane or in the bulk solution. The two distinct features become more evident when we calculate their relative enhancement factors (details in the *SI Appendix*). The enhancement factor of Pb^{2+} for the MoS_2-COOH membrane is the only case with a value above 1 (up to 1.4). Remarkably, we observed that ions with the largest $\boldsymbol{P}_i$, i.e., $K^+/Pb^{2+}/Na^+$, show concentration crossovers between the feed and permeate in the long-term test (*SI Appendix*, Fig. S8), while there are concentration equilibria for ions with second largest $\boldsymbol{P}_i$, i.e., Li^+/Cu^{2+}, and concentration disequilibria for other ions with smaller $\boldsymbol{P}_i$. The crossover of ions with the largest $\boldsymbol{P}_i$ is driven by the tendency toward global equilibrium across the membrane, as evidenced by the gradual decrease of osmotic pressure (*SI Appendix*, Fig. S9).

The transmembrane transport behavior of ions was also evaluated after removing the fastest one (K^+) or the anomalous one (Pb^{2+}). Upon removing K^+, Pb^{2+} still shows anomalously enhanced transport and becomes the fastest ion (*SI Appendix*, Fig. S10). After removing Pb^{2+}, the overall transport trend is consistent (*SI Appendix*, Fig. S11). Additionally, when the anions in the mixture solution are changed from Cl^--dominated ones (Cl^-/NO_3^-) to pure NO_3^-, the distinct ion transport features within the MoS_2-COOH membrane are preserved, although the two anion systems show differences in the absolute ratio values (*SI Appendix*, Fig. S12). This difference might indicate different cation–anion pairings as theoretically predicted (7), which needs further investigation. Moreover, such anomalous enhancement cannot be observed in the commercial Nafion™-perfluorinated membrane (Nafion™ 117), which primarily conducts monovalent cations (*SI Appendix*, Fig. S13). All these results indicate that the anomalous features are intrinsic transport properties of the metal cations across the 2D confined channels in the MoS_2-based membranes, especially for Pb^{2+} in the 2D confined MoS_2-COOH channels.

The second feature can be qualitatively understood within the framework of dehydration effects under confinement. When ion dehydration occurs under confined space, the energy penalties increase for ions with larger hydrated radius and greater hydration enthalpy, leading to decreased diffusion coefficients as compared to the bulk solution. This analysis can be supported by the exponential decrease of the mobilities of metal cations versus their hydration enthalpies that have been measured for channels with similar confined dimensions (18). However, the anomalously enhanced $\boldsymbol{P}_i$ of Pb^{2+} and Cu^{2+} in the MoS_2-based membrane cannot be explained using simple pictures of the influence of size effect or dehydration effects.

Ion-channel Interactions

To elucidate the origin of anomalous Pb^{2+} and Cu^{2+} transport, we conducted exhaustive analyses examining the thermodynamics regarding the binding between metal cations and MoS_2-based membranes. In particular, we focused on ion interactions with the channel surface to probe the effect of chemistry in confinement.

We first performed membrane uptake tests. In single ion uptake experiments using MoS_2-COOH channels, all the examined ions have considerable uptake following the order $Cu^{2+} > Pb^{2+} > Cd^{2+} > Mg^{2+} > K^+$ (Fig. 3*A* and *SI Appendix*, Fig. S14). However, in the mixed ion solution, both the pristine MoS_2 and MoS_2-COOH membranes have preponderant uptake of Pb^{2+} and Cu^{2+} and negligible uptake of other cations (Fig. 3 *B* and *C*), which deviate significantly from the single ion uptake results. Selective removal of Pb^{2+} and Cu^{2+} was also reported using suspended pristine MoS_2 sheets in a previous study (27). In the mixture solution uptake tests, the dominating ion was Cu^{2+} (~1.7 fold over Pb^{2+}) in the pristine MoS_2 channels, which changed to Pb^{2+} (~threefold over Cu^{2+}) in the MoS_2-COOH channels. This comparison is robust to changes of the anions, pH, and concentration of the mixture solution (*SI Appendix*, Figs. S15 and S16). The observed change corroborates the significant role of chemical environment in angstrom-scale channels to ion binding. Based upon the above systematic studies, we conclude that the anomalously enhanced transport of Pb^{2+} and Cu^{2+} arises from their strong interactions in the MoS_2-based membranes over others, which thereby translate into huge thermodynamic advantages in their transport across the membrane. However, kinetics also plays an important role in the results, as we discuss later.

Additionally, high-angle annular dark-field scanning transmission electron microscopy (HAADF-STEM) imaging confirms that the adsorbed cations show single-site populations in the membrane, as represented by the bright dots partly encircled in Fig. 3 *D* and *E*. Pair distribution function analyses indicate that Cu^{2+} or Pb^{2+} does not change the basic framework of either MoS_2 or MoS_2-COOH membranes, while modifying local and intermediate structures (*SI Appendix*, Fig. S17).

To experimentally confirm the role of the carboxylate group, we used infrared (IR) vibrational spectroscopy to probe the interactions between metal cations and the carboxylate groups. MoS_2-COOH membranes were soaked with single metal cation salt solutions (1 M in D_2O), and then the vibrational absorption spectra of the carboxylate group were measured. In the absorption spectra (Fig. 4*A* and *SI Appendix*, Fig. S18), typically there are three characteristic peaks, the protonated (/deuterated) COOH(D) centered at ~1,710 cm^{-1}, the fully hydrated COO^- centered at ~1,615 cm^{-1}, and the emergent peak due to the coordination between COO^- and metal cations COO^---M^{n+} ranging from 1,550 to 1,590 cm^{-1} (28, 29). Clearly, the MoS_2-COOH membrane soaked with pure D_2O only shows a dominant COOH(D) peak and a weak COO^- peak. MoS_2-COOH membranes treated with KCl or LiCl have almost the same absorption spectra as the pure D_2O-treated one, suggesting weak interactions between monovalent alkali cations and the COO^- group, with no observable coordination. However, upon being soaked in the divalent and trivalent cation solutions, MoS_2-COOH membranes show a reduced COOH(D) peak, an increased free COO^- peak, and an emergent COO^---M^{n+} coordination peak. The COO^---M^{n+} coordination peak is of spectroscopic interest particularly because its redshift degree can be used to infer the binding motif (monodentate versus bidentate) and strength of coordination between COO^- and metal cations (29). The coordination peak information is summarized in Fig. 4*B*. The COO^---Pb^{2+} coordination peak shows the largest redshift degree and the absorption spectrum of the

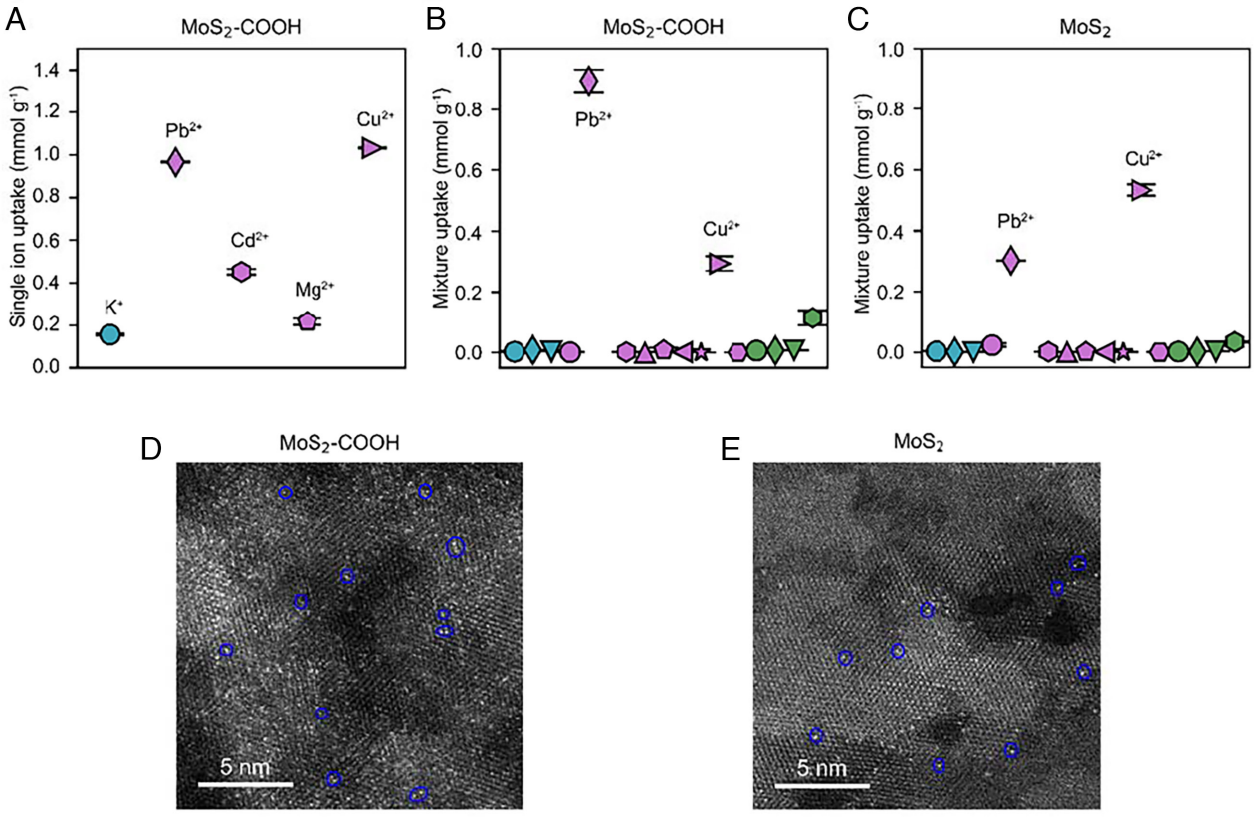

Fig. 3. Ion uptake in the 2D channels. (*A*) Uptake by the MoS_2-COOH membranes in the single ion solution (~4 mM). (*B* and *C*) Uptake by the pristine MoS_2 membrane and the MoS_2-COOH membrane in the mixed ions solution, respectively. Ion labels in *B* and *C* from left to right are K^+/Na^+/Li^+/Ba^{2+}/Pb^{2+}/Ca^{2+}/Cd^{2+}/Mn^{2+}/Mg^{2+}/Zn^{2+}/Co^{2+}/Cu^{2+}/Ni^{2+}/La^{3+}/Y^{3+}/Yb^{3+}/Al^{3+}, which are the same as those in Fig. 2*A*. (*D* and *E*) HAADF-STEM image of the MoS_2-COOH membrane and the MoS_2 membrane after ion uptake in the mixture solution, respectively. Blue circles represent the adsorbed single-site cations. Mixture: ~ 4 mM, Cl^-/NO_3^- (~96 mM:44 mM) anions, pH ~ 4.13.

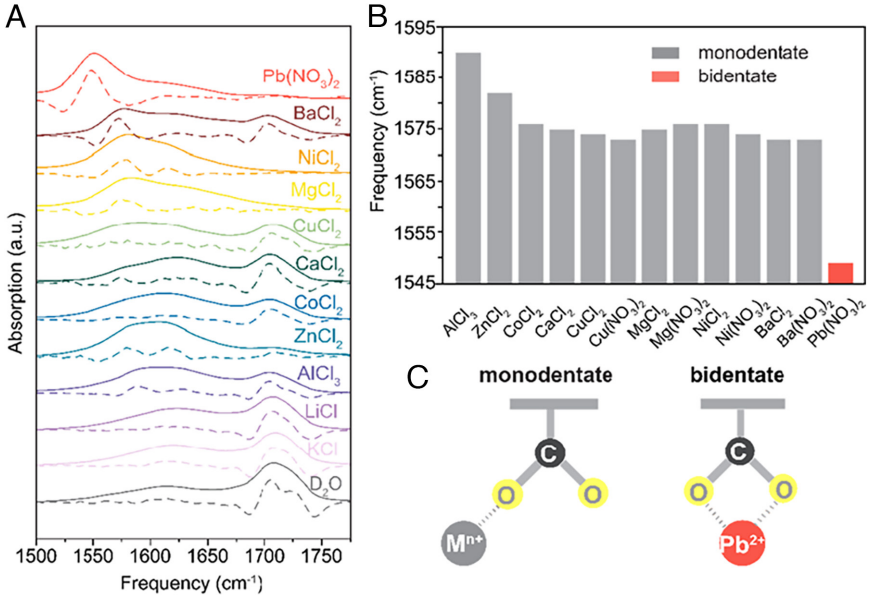

Fig. 4. Ion-functional group interactions. (*A*) The effect of different metal cations on the IR absorption spectra of the carboxylate group in the MoS_2-COOH membranes. The dashed lines are the corresponding negative second-order derivatives of the absorption spectra (solid lines) for peak pinpointing. (*B*) The peak frequency of the coordinated COO^---M^{n+} complexes extracted from *A*. (*C*) Schematic illustrations of the monodentate and bidentate coordination mode between metal cations and carboxylate group.

MoS_2-COOH membrane shows a dominant COO^---Pb^{2+} coordination peak with minimal COOH(D) peak and COO^- peak, further emphasizing the coordination strength. Based on the peak position (29), it can also be inferred that Pb^{2+} uniquely adopts a bidentate coordination mode with COO^-, while other divalent and trivalent cations adopt a monodentate complexation mode, as schematically illustrated in Fig. 4*C*.

Density functional theory (DFT) calculations were then conducted to investigate the binding strength and configuration of both Cu^{2+} and Pb^{2+} in the MoS_2-COOH channels. Detailed discussions of DFT calculations are provided in *SI Appendix*, Text. The results show that the binding mode of Cu^{2+} to carboxylate groups is monodentate (Fig. 5 *B* and *C*) while Pb^{2+} is bidentate (Fig. 5 *E* and *F*) in our calculations, which is consistent with the experimental FTIR results. The result also indicates that the introduction of 2D confinement can significantly increase the binding energy (BE) of Cu^{2+} (~0.33 eV, Fig. 5 *B* and *C*) and Pb^{2+} (~0.58 eV, Fig. 5 *E* and *F*). It is noteworthy that the Cu^{2+} interacts strongly with S (*SI Appendix*, Fig. S19). This contrasts with Pb^{2+}, which shows negligible interaction with sulfur and the binding energy is more determined by the bidentate coordination with the acetate (*SI Appendix*, Fig. S19). The Cu^{2+}-sulfur interaction is stronger than the bidentate binding of Pb^{2+}, and this leads to binding strength for Cu^{2+} that is stronger than that for Pb^{2+} in the MoS_2-COOH channels (Fig. 5 *C* and *F*). The binding energies in the DFT calculations are fully consistent with the experimental single salt uptake results that Cu^{2+} has a larger uptake than Pb^{2+} in the MoS_2-COOH membrane (Fig. 3*A* and *SI Appendix*, Fig. S14).

Ion Interplay in the Pb^{2+}-defined MoS_2-COOH Channels

Further data analysis highlights an obvious flip in the MoS_2-COOH channels: As mentioned above, the DFT calculations show that binding energy of Cu^{2+} is greater than that of Pb^{2+} in the MoS_2-COOH channels (Fig. 5 *C* and *F*), while the single ion uptake tests also confirm that Cu^{2+} has a greater uptake than Pb^{2+} in the MoS_2-COOH channels (Fig. 3*A* and *SI Appendix*, Fig. S14). However, Pb^{2+} shows a ~three to sevenfold greater uptake than Cu^{2+} in the mixture uptake tests (Fig. 3*B* and *SI Appendix*, Fig. S15). This flip of uptake order between Pb^{2+} and Cu^{2+} in the MoS_2-COOH channels is further confirmed in the uptake tests in the binary Cu^{2+}/Pb^{2+} mixture solution (*SI Appendix*, Fig. S20). By comparison, this flip does not exist in the pristine MoS_2 channels (Fig. 3*C* and *SI Appendix*, Figs. S16, S20, and S21). Thus, the flip indicates a more complicated picture of ion interplay in the chemically functionalized 2D channels, which remains a puzzle to be understood.

To unravel this puzzle, we first characterized the microstructure of the 2D channels after ion uptake using X-ray diffraction (XRD). MoS_2-COOH membranes show unique diffraction characteristics with single ion uptake corresponding to different uptake levels and binding strengths (Fig. 6*A* and *SI Appendix*, Fig. S22). For example, the (004) peak is prominent in the Pb^{2+}/Cu^{2+}/Cd^{2+}-treated membranes, weakly present in the Mg^{2+}-treated one, while totally absent in the DI water/K^+/Al^{3+}-treated ones. The order of interlayer spacings of MoS_2-COOH membranes with single ion uptake is as follows: K^+(11.1 Å) < Pb^{2+} (11.4 Å) < Cu^{2+} (11.9 Å) < Cd^{2+} (12.0 Å) < Al^{3+} (12.6 Å) < Mg^{2+} (14.8 Å). We note that similar results were also reported in graphene oxide membranes (30). Moreover, we found that the Pb^{2+}-treated MoS_2-COOH membrane shows the best layer-to-layer structure indicating better arrangement of water molecules and cations in the MoS_2-COOH channels in the wet state, as proven by its largest value of I(004)/I(002) and narrowest full width at half maximum (*SI Appendix*, Table S2). Furthermore, we observed that the diffraction spectrum of the MoS_2-COOH membranes in the mixture solution is basically defined ("locked") by Pb^{2+}, as indicated by the position and intensity ratio of the peaks (*SI Appendix*, Table S2). The interlayer spacing change could also explain why Cu^{2+} has smaller uptake in the mixture than Pb^{2+} in the MoS_2-COOH membrane despite Cu^{2+} having both greater uptake in the single ion test and larger binding energy in DFT calculations:

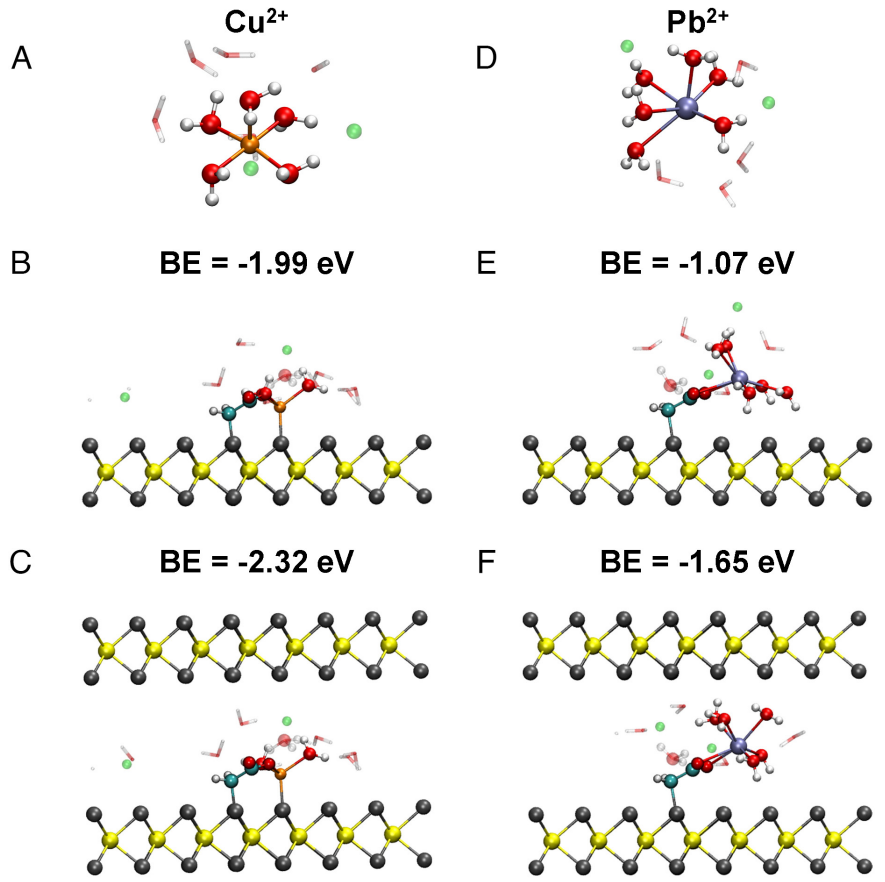

Fig. 5. DFT calculations of the optimized structure and the corresponding binding energies for Cu^{2+} and Pb^{2+} in the MoS_2-COOH systems. (*A–C*) Cu^{2+} ion in the bulk solution, bound to monolayer and bilayer MoS_2-COOH, respectively. (*D–F*) Pb^{2+} ion in the bulk solution, bound to monolayer and bilayer MoS_2-COOH, respectively. BE: binding energy. Mo is represented in yellow, S in gray, C in cyan, O in red, H in white, Cl in green, Cu in orange, and Pb in ice blue.

Since Pb^{2+} can lock the interlayer spacing at a smaller value than is appropriate for Cu^{2+}, the kinetic energy barrier for Cu^{2+} uptake increases (*SI Appendix*, Fig. S23) (31). In addition, this interlayer change also means that Cu^{2+} might be pushed out of its thermodynamically stable states in the MoS_2-COOH channels when Pb^{2+} is present. Both the kinetic and thermodynamic factors mentioned

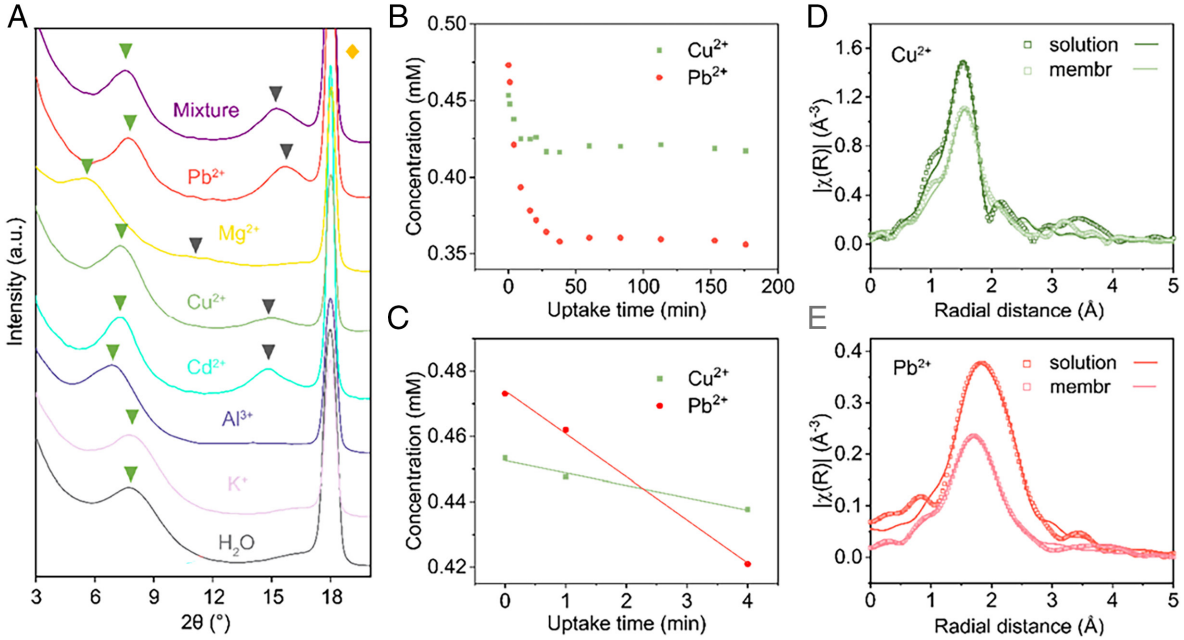

Fig. 6. Pb^{2+} defines the structure of MoS_2-COOH channels. (*A*) The XRD spectra of the MoS_2-COOH membranes treated by different single-ion solutions (~4 mM, natural pH after salt dissolving) and mixed ions solution. The green triangle, grey triangle, and orange parallelogram indicate the (002), (004) peak of the MoS_2-COOH membrane and that of the PTFE membrane, respectively. (*B*) The concentration profile of Cu^{2+} and Pb^{2+} in the solution throughout the test. (*C*) is the zoom-in plot of *B* showing that the uptake of Pb^{2+} is faster than Cu^{2+} (slope ratio Pb^{2+}:Cu^{2+} = 3.5:1). (*D* and *E*) Fourier-transformed EXAFS spectra of Cu^{2+} and Pb^{2+} in the bulk solution and in the MoS_2-COOH membrane, respectively.

above could lead to the reduced uptake of Cu^{2+} in the MoS_2-COOH when in the presence of Pb^{2+}.

Then, a question rises naturally: Why Pb^{2+}, rather than Cu^{2+}, can define the interlayer spacing of MoS_2-COOH in the mixture? To approach this question, we examined the uptake kinetics of the mixed ions in the MoS_2-COOH membrane. Here, we put the MoS_2-COOH membrane in the mixture solution and monitored the ion concentration change in the solution with respect to time (more details in *SI Appendix*). The full results are presented in *SI Appendix*, Fig. S23. This shows that only Cu^{2+} and Pb^{2+} show appreciable decrease of concentration in the mixture solution (Fig. 6*B*), while other ions show negligible changes (*SI Appendix*, Fig. S24). The result is consistent with the uptake results (Fig. 3*B* and *SI Appendix*, Fig. S15). Besides, we found that the uptake kinetics of Pb^{2+} is ~3.5-fold faster than that of Cu^{2+} (Fig. 6*C*). Extended X-ray absorption fine structure (EXAFS) analyses show that ~one or two water molecules are removed from Pb^{2+} and Cu^{2+} in their first hydration shell in the MoS_2-COOH membrane, as compared to their bulk solutions (Fig. 6 *D* and *E* and *SI Appendix*, Fig. S25 and Table S3). Given the fact that Pb^{2+} has a much weaker interaction with water molecules in the hydration shell than Cu^{2+} (hydration enthalpies: −1,480 of Pb^{2+} vs. −2,100 kJ/mol of Cu^{2+}), the faster uptake kinetics of Pb^{2+} can be presumably attributed to the smaller dehydration energy barrier of Pb^{2+} in the channel. Thus, our results indicate a complicated interplay between kinetic and thermodynamic factors for ions in 2D confinement, which calls for more attention in future study.

To conclude, through the investigation of uptake and competitive ion transport, we provide a holistic picture describing ion binding and transport under angstrom-scale confinement and reveal new details of ion interplay in the confined channels. Our method can be extended to study the role of more sophisticated chemistry in similarly confined environments, which is beneficial to the design of single-ion selective membranes and devices thereof.

Data, Materials, and Software Availability. All study data are included in the article and/or *SI Appendix*.

ACKNOWLEDGMENTS. This work is supported by Advanced Materials for Energy-Water-Systems Center, an Energy Frontier Research Center funded by the U.S. Department of Energy, Office of Science, Basic Energy Sciences. This work made use of instruments in the Electron Microscopy Core of UIC's Research Resources Center. This research used resources of the Advanced Photon Source, a U.S. Department of Energy (DOE) Office of Science user facility operated for the DOE Office of Science by Argonne National Laboratory under Contract No. DE-AC02-06CH11357.

Author affiliations: [a]Pritzker School of Molecular Engineering, University of Chicago, Chicago, IL 60637; [b]Department of Chemistry, Northwestern University, Evanston, IL 60208; [c]Department of Chemistry, SRM Institute of Science and Technology, Kattankulathur, Tamil Nadu 603203, India; [d]Department of Chemistry, Institute for Biophysical Dynamics, and James Franck Institute, University of Chicago, Chicago, IL 60637; [e]X-Ray Science Division, Advanced Photon Source, Argonne National Laboratory, Lemont, IL 60439; [f]Advanced Materials for Energy-Water Systems Energy Frontier Research Center and Chemical Sciences and Engineering Division, Argonne National Laboratory, Lemont, IL 60439; and [g]Electron Microscopy Core, University of Illinois Chicago, Chicago, IL 60607

1. A. C. Dolphin, P. A. Insel, T. F. Blaschke, U. A. Meyer, Introduction to the theme "ion channels and neuropharmacology: From the past to the future". *Annu. Rev. Pharmacol. Toxicol.* **60**, 1–6 (2020).
2. A. Siria, M.-L. Bocquet, L. Bocquet, New avenues for the large-scale harvesting of blue energy. *Nat. Rev. Chem.* **1**, 1–10 (2017).
3. K. Xiao, L. Jiang, M. Antonietti, Ion transport in nanofluidic devices for energy harvesting. *Joule* **3**, 2364–2380 (2019).
4. X. Qian *et al.*, $CdPS_3$ nanosheets-based membrane with high proton conductivity enabled by Cd vacancies. *Science* **370**, 596–600 (2020).
5. J. R. Werber, C. O. Osuji, M. Elimelech, Materials for next-generation desalination and water purification membranes. *Nat. Rev. Mater.* **1**, 1–15 (2016).
6. Y. Xue *et al.*, Atomic-scale ion transistor with ultrahigh diffusivity. *Science* **372**, 501–503 (2021).
7. P. Robin, N. Kavokine, L. Bocquet, Modeling of emergent memory and voltage spiking in ionic transport through angstrom-scale slits. *Science* **373**, 687–691 (2021).
8. D. A. Doyle *et al.*, The structure of the potassium channel: Molecular basis of K^+ conduction and selectivity. *Science* **280**, 69–77 (1998).
9. Y. Zhou, J. H. Morais-Cabral, A. Kaufman, R. MacKinnon, Chemistry of ion coordination and hydration revealed by a K+ channel–Fab complex at 2.0 Å resolution *Nature* **414**, 43–48 (2001).
10. Y. Jiang *et al.*, The open pore conformation of potassium channels. *Nature* **417**, 523–526 (2002).
11. R. H. Tunuguntla *et al.*, Enhanced water permeability and tunable ion selectivity in subnanometer carbon nanotube porins. *Science* **357**, 792–796 (2017).
12. E. Secchi *et al.*, Massive radius-dependent flow slippage in carbon nanotubes. *Nature* **537**, 210–213 (2016).
13. C. Duan, A. Majumdar, Anomalous ion transport in 2-nm hydrophilic nanochannels. *Nat. Nanotechnol.* **5**, 848–852 (2010).
14. T. Jain *et al.*, Heterogeneous sub-continuum ionic transport in statistically isolated graphene nanopores. *Nat. Nanotechnol.* **10**, 1053–1057 (2015).
15. J. Feng *et al.*, Observation of ionic Coulomb blockade in nanopores. *Nat. Mater.* **15**, 850–855 (2016).
16. J. Shen *et al.*, Fast water transport and molecular sieving through ultrathin ordered conjugated-polymer-framework membranes. *Nat. Mater.* **21**, 1183–1190 (2022).
17. J. Shen, G. Liu, Y. Han, W. Jin, Artificial channels for confined mass transport at the sub-nanometre scale. *Nat. Rev. Mater.* **6**, 294–312 (2021).
18. A. Esfandiar *et al.*, Size effect in ion transport through angstrom-scale slits. *Science* **358**, 511–513 (2017).
19. K. Gopinadhan *et al.*, Complete steric exclusion of ions and proton transport through confined monolayer water. *Science* **363**, 145–148 (2019).
20. T. Mouterde *et al.*, Molecular streaming and its voltage control in ångström-scale channels. *Nature* **567**, 87–90 (2019).
21. B. Radha *et al.*, Molecular transport through capillaries made with atomic-scale precision. *Nature* **538**, 222–225 (2016).
22. S. Y. Noskov, S. Bernèche, B. Roux, Control of ion selectivity in potassium channels by electrostatic and dynamic properties of carbonyl ligands. *Nature* **431**, 830–834 (2004).
23. E. R. Nightingale, Phenomenological theory of ion solvation. Effective radii of hydrated ions. *J. Phys. Chem.* **63**, 1381–1387 (1959).
24. E. Hoenig *et al.*, Controlling the structure of MoS2 membranes via covalent functionalization with molecular spacers. *Nano Lett.* **20**, 7844–7851 (2020).
25. Z. Wang *et al.*, Understanding the aqueous stability and filtration capability of MoS_2 membranes. *Nano Lett.* **17**, 7289–7298 (2017).
26. L. Ries *et al.*, Enhanced sieving from exfoliated MoS 2 membranes via covalent functionalization. *Nat. Mater.* **18**, 1112–1117 (2019).
27. Z. Wang *et al.*, Superselective removal of lead from water by two-dimensional MoS_2 nanosheets and layer-stacked membranes. *Environ. Sci. Technol.* **54**, 12602–12611 (2020).
28. J. W. DePalma, P. J. Kelleher, L. C. Tavares, M. A. Johnson, Coordination-dependent spectroscopic signatures of divalent metal ion binding to carboxylate head groups: H 2 - and He-tagged vibrational spectra of M 2+ ·RCO 2 $^-$ (M = Mg and Ca, R = −CD 3, −CD 2 CD 3) complexes. *J. Phys. Chem. Lett.* **8**, 484–488 (2017).
29. C. C. R. Sutton, G. da Silva, G. V. Franks, Modeling the IR spectra of aqueous metal carboxylate complexes: Correlation between bonding geometry and stretching mode wavenumber shifts. *Chem. Eur. J.* **21**, 6801–6805 (2015).
30. L. Chen *et al.*, Ion sieving in graphene oxide membranes via cationic control of interlayer spacing. *Nature* **550**, 380–383 (2017).
31. R. Epsztein, R. M. DuChanois, C. L. Ritt, A. Noy, M. Elimelech, Towards single-species selectivity of membranes with subnanometre pores. *Nat. Nanotechnol.* **15**, 426–436 (2020).